AIAA Propulsion and Energy Forum
19-22 August 2019, Indianapolis, IN
AIAA Propulsion and Energy 2019 Forum

10.2514/6.2019-4303

Modeling of Hybrid-Electric Powertrain for Unmanned Aerial Systems

Darren Dehesa[1] and Shyam Menon[2]

Louisiana State University, Baton Rouge, LA, 70808

Hybrid-Electric aircraft powertrain modeling for Unmanned Aerial Systems (UAS) is a useful tool for predicting powertrain performance of the UAS aircraft. UAS aircraft utilize small-displacement engines that have poor thermal efficiency and as a result, could benefit from a hybridized powertrain by reducing fuel consumption. The scope of this work aims to provide a tool that can allow one to estimate the hybrid powertrain performance based upon the aircraft specifications, component specifications, propulsion component performance maps, and mission power profiles. Utilizing MATLAB, a powertrain model will be developed that can facilitate system performance testing for a given mission profile, as well as component sizing which will allow for optimized powertrain power consumption in addition to aircraft range and endurance

I. Introduction

The desire to reduce vehicle greenhouse gas emissions from fossil fuel-based propulsion systems has created an increasing interest in hybrid aircraft technology. This reduction in fossil fuel usage is mainly accomplished by introducing more electrified forms of propulsion into vehicles. A hybrid vehicle is any vehicle that implements two distinct forms of power used for propelling the vehicle. Many different forms of hybrid systems have mainly been used in automobiles such as petroleum-electric hybrid or fuel cell-electric hybrid systems which achieve a significant reduction in fuel consumption. The success of hybrid systems in automobiles has created interest in creating hybrid aircraft systems. Research performed by Schömann [1] on hybrid powertrain development focused on the accuracy, high computational efficiency, and generic applicability of modeling a hybrid powertrain's performance. Schömann analyzed the effect that the electric flight time had on the hybrid aircraft weight and fuel consumption. He found that as one increases the electric flight time or ratio of electric flight time to the total flight time of the hybrid system, the take-off mass of the aircraft increases. This is because of the increased battery mass required to achieve higher flight times, which then makes the aircraft infeasible [1]. Schömann determined that for an aircraft with a required flight time of 5h 30min or less, a flight time ratio of 0.25 provides optimal fuel efficiency. For flight time ratios from 0.50-0.75, the only benefit of hybridization is to have one of the propulsion units act as a power booster for climbing segments or high-power demand periods.

Many hybrid propulsion systems are petroleum-electric based because of its simplicity and ease of integration. Three different powertrain configurations are possible, which are series, parallel, and split power. Each of these configurations have their pros and cons, such as increased packaging weight or reduced versatility. The series configuration (Figure 1a) is the simplest powertrain type consisting of electric motors (EM), batteries, and internal combustion (IC) engine with a generator. The series hybrid vehicle's propulsion is purely derived from electric motors, and an IC engine serves as an auxiliary source of power for the electric motor when the batteries require charging. The IC engine during charging periods operates at some optimum point to reduce fuel consumption. The parallel (Figure 1b) configuration, similar to the series configuration contains EM, batteries, and an IC engine. However, the parallel hybrid vehicle is a more complex powertrain type where EM and IC engine are coupled such that they can power the vehicle either individually or together. Parallel configurations usually contain a gearbox to couple the power

[1] Graduate Research Assistant, Mechanical and Industrial Engineering Department, ddehes1@lsu.edu
[2] Assistant Professor, Mechanical and Industrial Engineering Department, smenon@lsu.edu

from both EM and IC engine, which means that both motors must run at the same speed in dual power mode. Moreover, the parallel system can utilize a generator to charge the batteries like the series configuration. However, most hybrid systems seen in automobiles utilize other methods to recharge the batteries such as regenerative braking [2]. Lastly, the power-split (Figure 1c) configuration combines both aspects of the series and parallel systems. Power-split powertrains are similar to the series configuration and have a generator for supplemental power for EM and charging batteries. Also, the power from the IC engine and EM can be coupled together via a gearbox to provide propulsion for the vehicle similar to the parallel system. Ultimately the use of either configuration is dependent on vehicle usage and requirements.

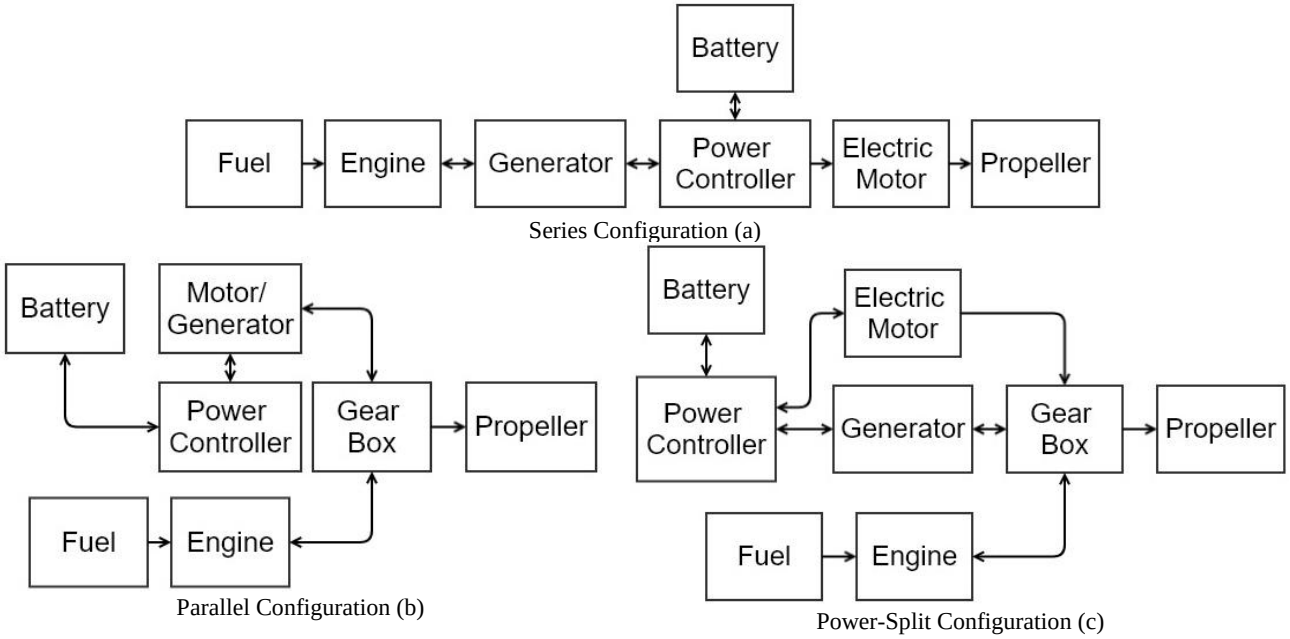

Figure 1 Hybrid Powertrain Configurations

Figure 2 Siemens series hybrid drive system [3]

Figure 3 Boeing Insitu ScanEagle UAV [4]

The interest in hybrid aircraft has slowly grown since automobiles implemented hybrid technology. Siemen's DA36 E-Star 2 plane (Figure 2) is a hybrid powertrain in development and uses a series configuration. Their series hybrid aircraft was able to complete a one-hour flight to the Paris Air Show in 2013, which claimed to reduce fuel consumption and emissions by 25% [3]. The goal for the aviation industry is to leverage the technology to reduce fuel consumption and emissions. However, some challenges exist which are unique to aircraft, one of which is weight. Because aircrafts have strict weight requirements, all the powertrain components of the aircraft must be chosen such that the performance of the aircraft is not hindered. Aircraft design aspects such as Gross Take-off Weight (GTOW),

payload weight, thrust, and lift are all important parameters that are linked together and affect performance. Therefore, when introducing a hybrid powertrain configuration into an aircraft, the components must be carefully selected for power, weight and efficient performance, so that the aircraft is able to perform the same or better than a conventional aircraft. The main source of weight in hybrid vehicles is the battery due to their low specific energy (~100-200 Wh/kg) [5]. When compared to gasoline, which has a specific energy of 45 MJ/kg, it is apparent that more battery mass is needed to match the energy capacity of most petroleum-based fuels. Higher energy density batteries (500-1500 Wh/kg) are under development, such as a lithium-sulfur battery with an energy density of 350 Wh/kg [6].

The concerns mentioned above about increased weight of aircraft with hybrid powertrains has motivated several groups to conduct studies on size and weight optimization [7]. These studies have focused their efforts on estimating the weight fractions of different hybrid powertrain configurations for use in a given unmanned aircraft with a fixed mission profile [8]. The previous studies generally pursued an iterative design approach which predicted sizes for the engine or the motor without particular regard to practically available components [9]. Further, the component performance was generally obtained from manufacturer specifications or scaling arguments. The current study is motivated by the specific need to improve the performance of a group 2 UAS by implementing a hybrid powertrain using off-the-shelf components. The low overall efficiency (4-18%) of the IC engine utilized in this UAS provides a key motivation to hybridize the powertrain [10]. This work aims to perform a comparative study of the performance of different hybrid powertrain configurations suitable for the particular UAS with a specified mission profile using measured performance data for the individual components of the powertrain. This will provide direct input to the UAS designers to aid in the selection of the powertrain. Beyond, predicting performance at fixed operating conditions, it is also desired to evaluate the dynamic performance of the powertrain during UAS flight. To this end, a dynamic system model is developed to simulate the performance of the hybrid powertrain using component performance maps as input to the program.

II. Methodology

Given the motivating aspects above, the development of a model incorporating performance maps of individual hardware components of the hybrid powertrain is valuable for estimating UAS performance. This work seeks to develop such a model, where a mission profile is used to simulate an operating scenario to predict the aircraft range in addition to the EM and IC engine power requirements necessary for steady level flight. MATLAB/Simulink is used to develop a model for a series hybrid configuration. Later efforts will include validation of the model using physical integrated component testing of the hybrid system as well as the modeling and testing of the more complex parallel and split power configurations.

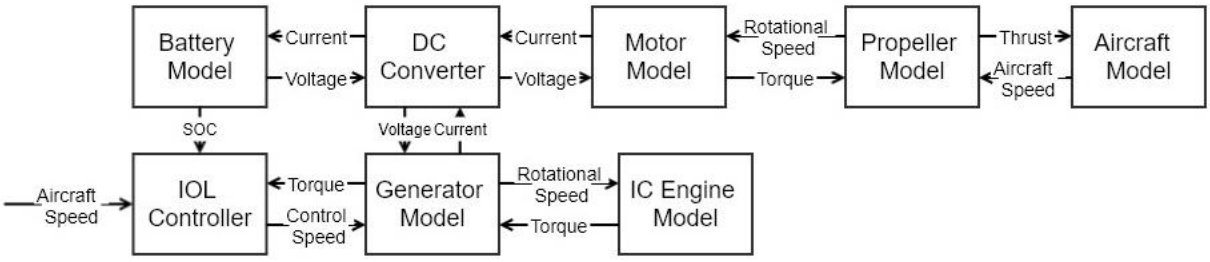

Figure 4 Series Hybrid layout and signal flow

The model shown in Figure 4 depicts the block diagram of the series hybrid powertrain model along with the signal flow of information. The model consists of multiple parts or blocks where each block represents the individual component models of the system. These blocks are created in Simulink and contain constitutive equations for each of the respective components required for the powertrain configuration. These equations will aim to characterize the power output or input for each essential component such as the IC engine, EM, or generator. A flight profile is created to simulate a mission for the aircraft, which includes speed and altitude data for a simple climb to cruise followed by

descent. The flight profile can be adapted as required to evaluate the performance of the powertrain and optimal power management schemes for different simulated missions. Performance is measured by comparing the hybrid aircraft range and endurance to that of the conventional aircraft using the model performance data for a given reference aircraft. The ScanEagle UAV is one of the reference aircraft used in the analysis, which will allow for a comparison of performance between the original and hybrid powertrain configuration. The aircraft powertrain is optimized for a configuration that achieves the best range with the optimal usage of power and least fuel consumption for a given mission profile.

III. System Model Description

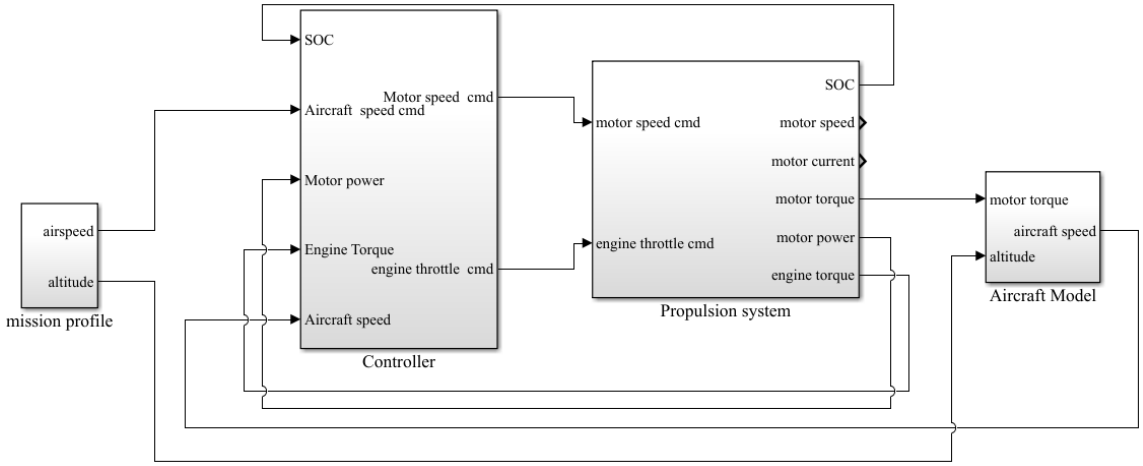

Figure 5 Series Hybrid model description

The model represented in Figure 5 depicts the full system model of the HEUAS, including the powertrain model, flight dynamics model, powertrain controller, and flight/mission profile used in the simulation. The model uses a forward-facing approach where information on the flight profile is passed to the powertrain controller which produces commands to send to the powertrain model. The series powertrain model then uses those input commands for requested speed, torque or throttle and outputs values for the torque or speed response depending on the component model. Those powertrain outputs are then passed to the aircraft model, which output the vehicle speed, which is used as one of the feedback signals for the powertrain controller. Next, each of the component models used in the development of the hybrid powertrain model is described in more detail.

A. Motor Model

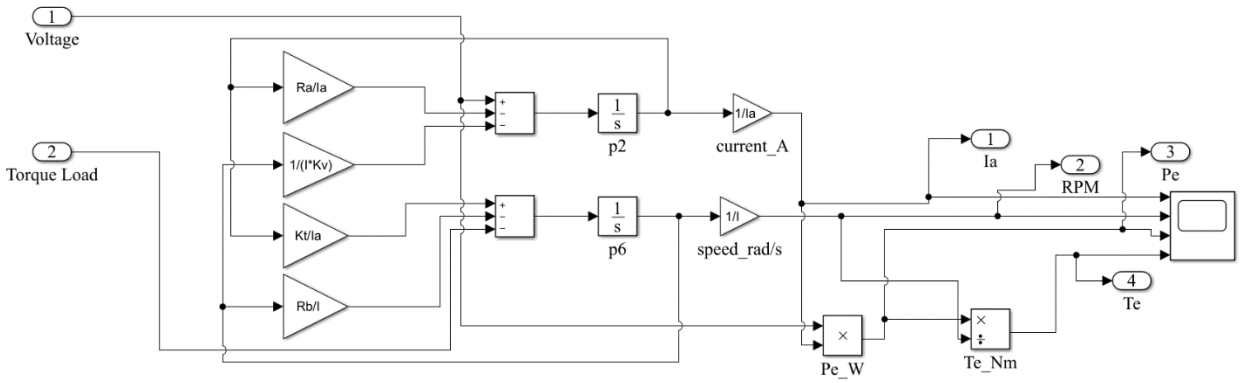

Figure 6 Electric Motor Model

The motor model utilizes a lumped parameter approach characterized by an equivalent circuit model for a permanent magnet DC motor, as shown in Figure 7. The mathematical equations used to model the motor are shown by Eq. (1)—(4) where the armature inductance (L), armature resistance (R), motor inertia (J), and viscous damping friction (b) are all parameters of the motor that characterize its performance including the back EMF constant K_b and the torque constant K_t. Proper parametrization of the motor is crucial for proper validation of the motor model. Thus, parameter identification will need to be performed where the various properties are determined experimentally for the motor in question.

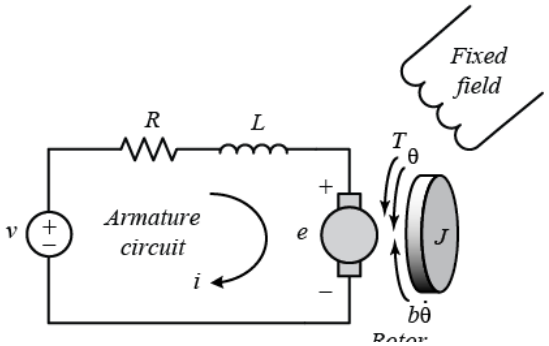

Figure 7 DC motor equivalent circuit model [16]

$$J\ddot{\theta} + b\dot{\theta} = K_t i \quad (1)$$

$$L\frac{di}{dt} + Ri = V - K_b\dot{\theta} \quad (2)$$

$$T = K_t i \quad (3) \qquad e = K_b\dot{\theta} \quad (4)$$

B. Generator Model

The generator model is fundamentally the same as the motor model however functionally the generator is run in reverse where all inputs to the generator are negative to signify the reverse operation which produces an opposing current for charging the battery. Like the motor model, parameter identification will also need to be performed to ensure that the model functions properly and can be validated. Also, the electrical system contains two dc to dc converters to regulate the voltage to the propulsive motor and the generator respectively, which was adapted from [11]. The bus side of converter for the motor is regulated to 60V while the generator is forced to provide a voltage

slightly higher than the battery to facilitate charging. The dc to dc converter model also models power loses modeled as a resistive load loss. The battery model is provided by Simscape power electronic block set and is a generic pre-defined battery model for a Li-Ion battery. With a nominal voltage of 24 V and a capacity of 100 Ah.

C. Engine Model

The engine model uses a throttle and speed input from the controller and the generator respectively. These inputs determine the torque output from the model, which is constructed using lookup tables for power as a function of speed at different throttle settings. A BSFC (Brake Specific Fuel Consumption) map that uses torque and speed inputs, provides fuel consumption data. This method of engine modeling was used for simplicity and speed of simulation. Moreover, given the significant differences in the architecture and operation of small two-stroke engines used in the UAS, as compared to conventional scale IC engines, there is a lack of confidence in the ability of standard IC engine models to be used in this work. The engine model also includes a fuel metering aspect or "fuel tank" where a set amount of fuel is specified for consumption to ensure that the model is not allowed to run when the entire set fuel amount is consumed. Then based upon the fuel usage, the fuel amount is reduced until it is fully consumed, at which point the torque output is forced to be zero signifying an out of fuel condition.

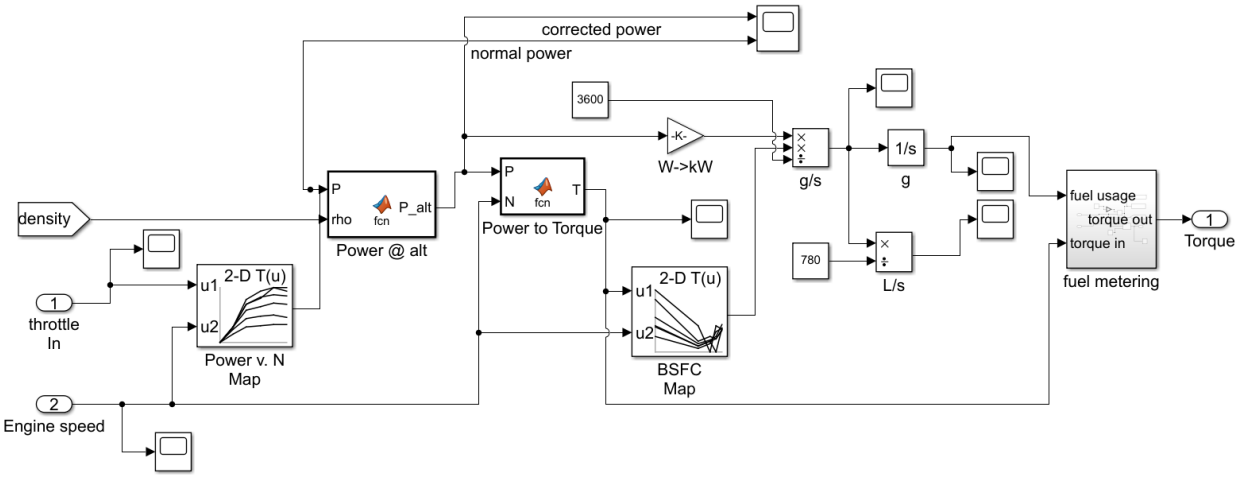

Figure 8 IC Engine model

D. Propeller Model

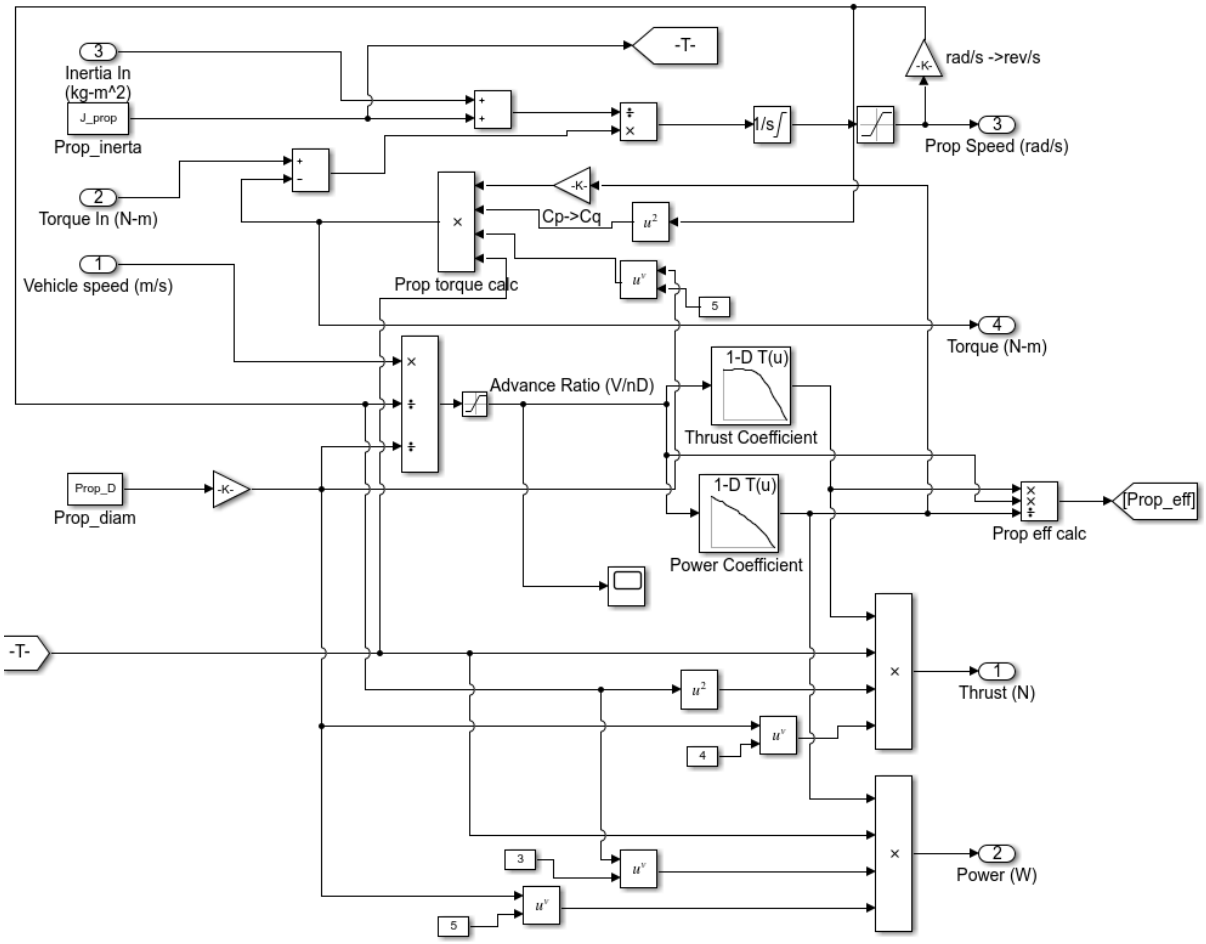

Figure 9 Propeller Model

The propeller model uses inputs of torque and aircraft speed to calculate the advance ratio *J* of the propeller (Eq. 5), which is then used as input to a lookup table for thrust and power coefficients for an 18x16 propeller. These coefficients are then used in Eq. (6) — (9) to calculate the thrust, power, and torque that the propeller requires for a given flight speed and torque input from the propulsive motor [12]. The torque input from the propulsive motor is used to calculate the propeller speed via integration the propeller acceleration based on a specified rotational inertia value. The output of the model is thrust, which is used later in the aircraft dynamics model to determine the aircraft speed.

$$J = \frac{V}{nD} \quad (5) \qquad C_Q = \frac{C_p}{2\pi} \quad (8)$$

$$C_T = \frac{T}{\rho n^2 D^4} \quad (6) \qquad C_Q = \frac{Q}{\rho n^2 D^5} \quad (9)$$

$$C_P = \frac{P}{\rho n^3 D^5} \quad (7)$$

E. UAS Model

The aircraft dynamics model used in this analysis is a simple point mass approximation that analyzes the sum of the forces acting on the aircraft. The model uses the thrust input from the propeller model to calculate the airspeed of

the aircraft. Equations (10) — (14) describe the vertical and horizontal forces on the aircraft that are used in the model. The model calculates the aircraft speed based on the thrust input then uses the speed and altitude information from the flight profile to calculate the flight angle [12]. The flight angle then allows for the calculation of the coefficient of lift, which is then used to determine the coefficient of drag using a lookup table for the lift-drag polar. The model in this simulation uses an aircraft weight of 18 kg which is equivalent to a group 2 UAS aircraft and the data for the lift-drag polar was provided by MATLAB code which calculates the lift-drag polar for the AAI Aerosonde UAV [13]. This simulation is a close approximation for UAS aircraft in this weight range.

$$T\sin\theta - D\sin\theta + L\cos\theta - W = m\frac{dV_v}{dt} \quad (10)$$

$$T\cos\theta - D\cos\theta - L\sin\theta = m\frac{dV_h}{dt} \quad (11)$$

$$C_l = \frac{L}{\frac{1}{2}\rho S_w V^2} \quad (12)$$

$$C_d = \frac{D}{\frac{1}{2}\rho S_w V^2} \quad (13)$$

$$\dot{h} = V\sin\theta \quad (14)$$

IV. HEUAS Control

The control strategy for the series hybrid system is depicted in Figure 10. The control strategy prioritizes minimum fuel consumption from the engine through an Ideal Operation Line (IOL) strategy adapted from [14]. The IOL strategy functions by tracking the minimum BSFC operation line shown in Figure 11. This is obtained by finding the minimum BSFC on various constant power lines. The implementation of the IOL controller starts with a lookup table of the ideal operating line to serve as a reference signal for the speed control based upon the torque output value from the engine model. The control loop will regulate the speed to the ideal operating speed, which should force the motor to operate in its most efficient region and provide enough power for the system. The power request from the ICE and generator system can vary because during the flight, the power required can change depending on the flight profile. Thus, in order to charge the battery, the ICE and generator system must provide the required propulsive power for the motor in addition to excess power for charging the battery when SOC falls below 60%. This control logic was adapted from [15] where a thermostat type of control approach is used to activate the controller when the threshold is reached. The controller must then determine the proper throttle value to determine the power or torque required from the ICE to charge the battery, which can be achieved at different operating points for throttle and speed values.

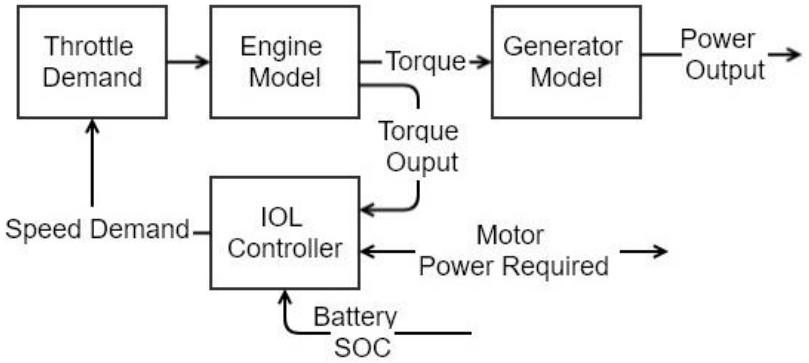

Figure 10 IOL controller diagram

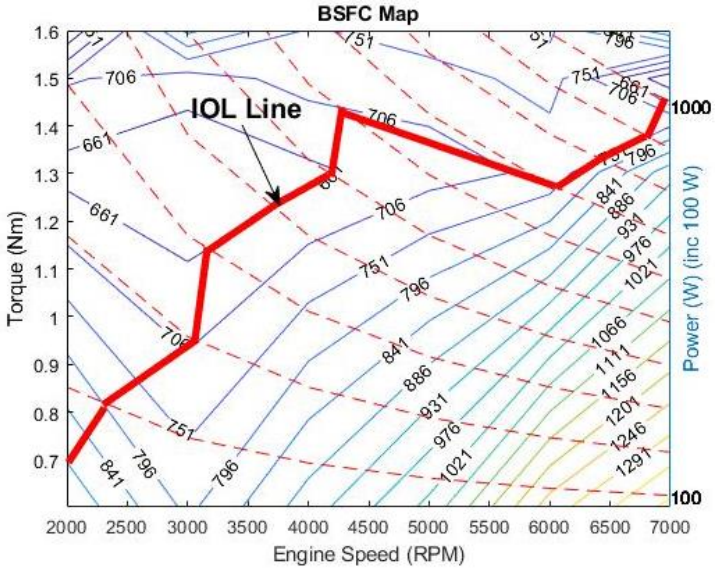

Figure 11 BSFC map with IOL line [10].

V. Simulation Results

The flight profile in Figure 12 and Figure 13 was created to simulate 30 minutes of flight time. A short take-off segment is followed by a climbing segment where the aircraft will climb at a rate of approximately 3.9 m/s or 770 ft/min at a speed of 30 m/s. After the climbing segment, the aircraft enters the cruise segment. During the cruise segment the aircraft also undergoes two different speed changes where it decelerates from the 35 m/s steady-state cruise speed to approximately 30 m/s then further decelerates to 24 m/s which is used to test the aircraft speed controller's ability to correct the speed change and to simulate changes in propulsion power demand. Figure 13 also plots the actual aircraft speed attained during the simulation. It can be seen that the desired and actual aircraft speeds almost exactly overlap each other. This shows that the controller manages to maintain the desired aircraft speed by controlling the electric motor-propeller unit with exception to the one spike at 700 s which corresponds to the battery reaching the SOC threshold to activate the engine-generator system. It should be noted the descent segment was neglected for the flight profile to restricted the performance analysis to the climbing and cruise segments. The climbing and cruising segments are deemed more important because aircraft undergo the highest power usage during climb and then continue to utilize most of the remaining energy during cruise. Moreover, aircraft descents are low power gliding descents. Thus, analyzing the propulsive power demand during this phase is not as crucial as take-off, climbing, and cruising segments.

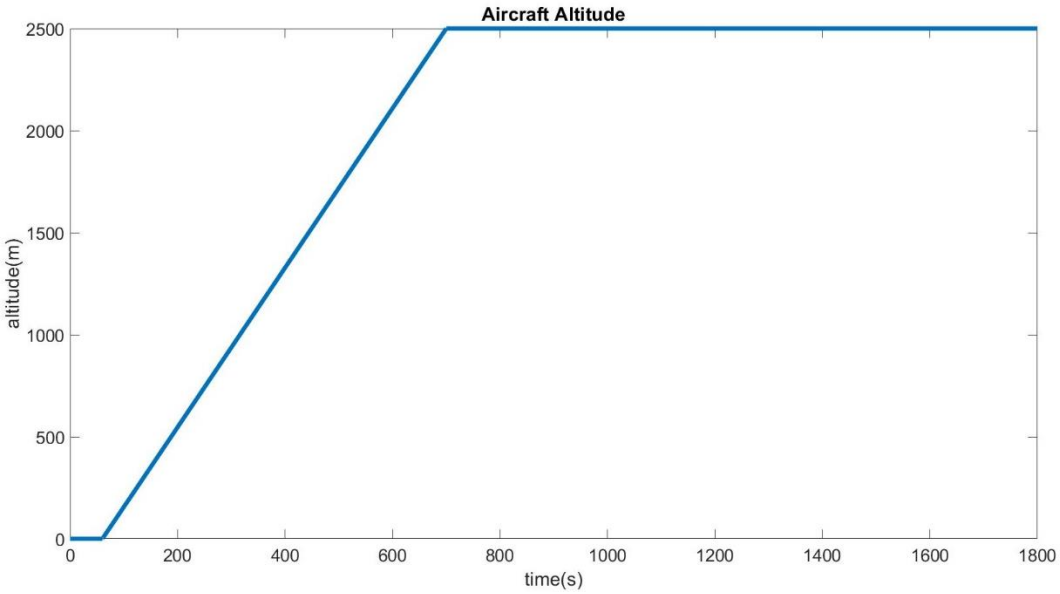

Figure 12 Altitude profile

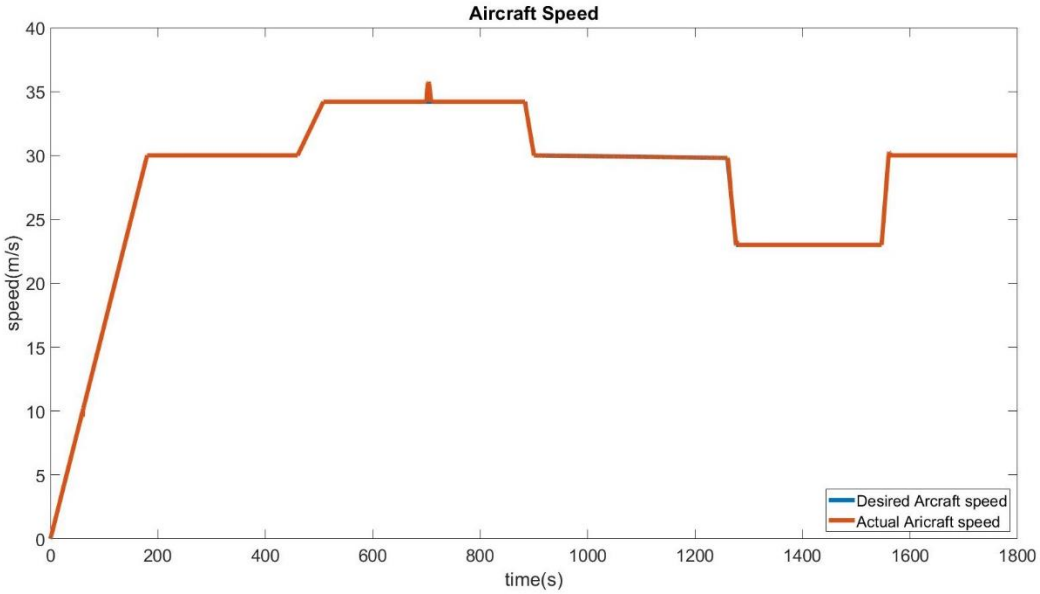

Figure 13 Aircraft speed profile

Figure 14 plots three quantities related to the battery as a function of time. This includes the state of charge (SOC) of the battery and its current and voltage outputs. As shown in Figure 14, the battery state of charge decreases from an initial value of 70% to the threshold value during the flight simulation. This initial SOC was chosen so that the aircraft would reach the threshold SOC before the 30 min flight time simulation was complete. If the initial SOC had been greater than 70%, then the engine-generator system would likely not be activated at all. This same effect could be achieved at a higher SOC by reducing the battery capacity, which was set at 100 Ah for this simulation. Once the SOC reaches the threshold value of 60%, the controller is able to hold the SOC constant for the remainder of the flight. This result indicates that the controller is regulating the state of charge to the desired value. This control logic can be modified so that the state of charge can be regulated at a higher SOC or more sophisticated control logic can be implemented to regulate over a range of SOC. The battery current in Figure 15 shows some large current spikes which are transient effects at the points where the generator is responding to speed changes of the IC engine due to the IOL

controller attempting to regulate the SOC and power demand. Corresponding spikes are also seen in the voltage profile. Generally, the battery current during the cruise portion of the flight is stabilized at 28A and voltage at 25V if no charging occurs. However, since charging began at the beginning of the cruise portion, the power is being supplied by the generator system and not the battery. Thus, these spikes are also a result of the aircraft speed change, which causes current spikes during these transitions. Note that the battery voltage here is DC voltage.

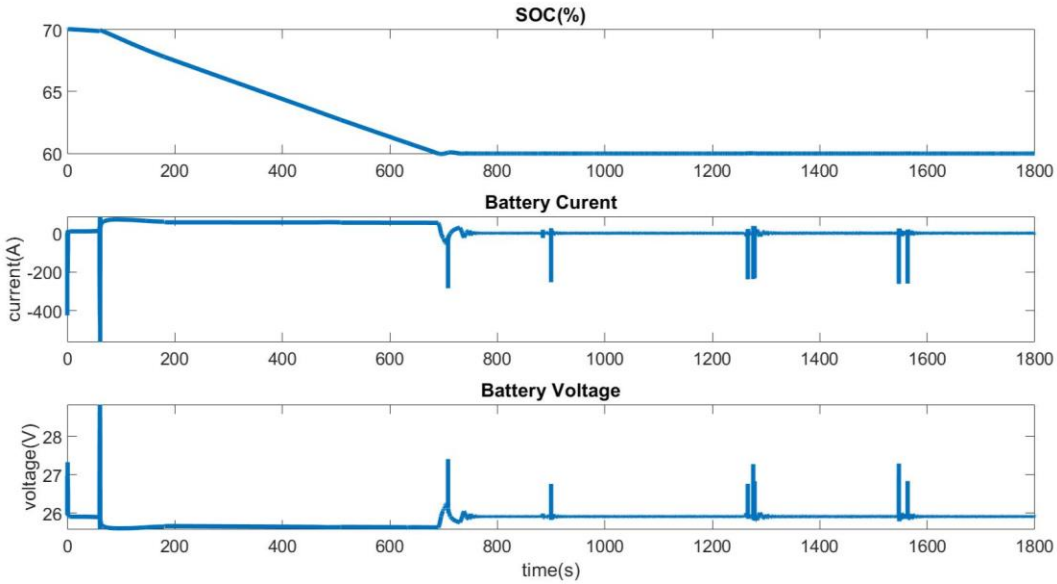

Figure 14 Battery model results

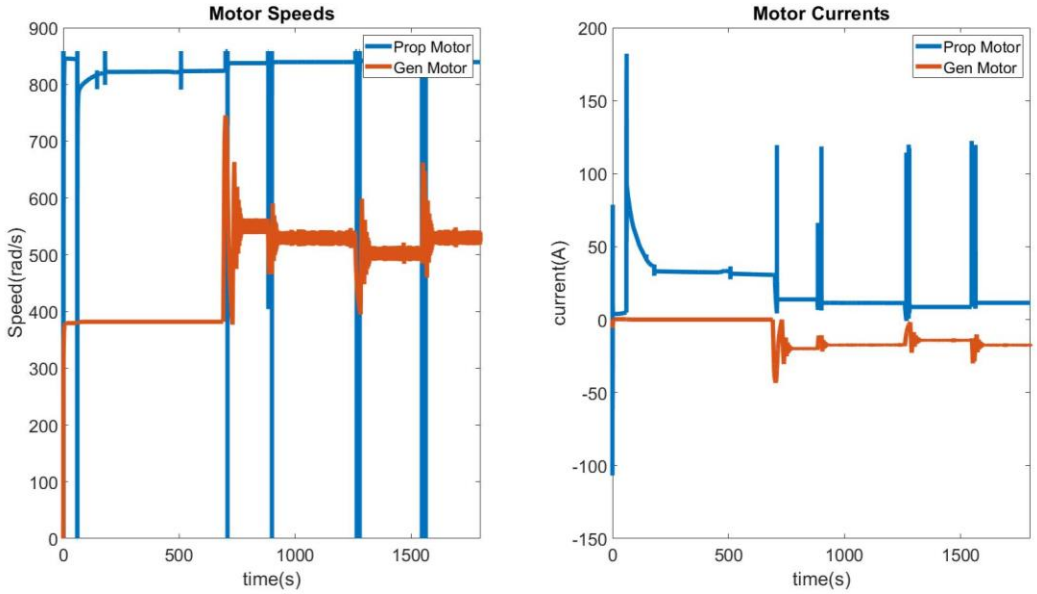

Figure 15 Motor/Generator current and speed results

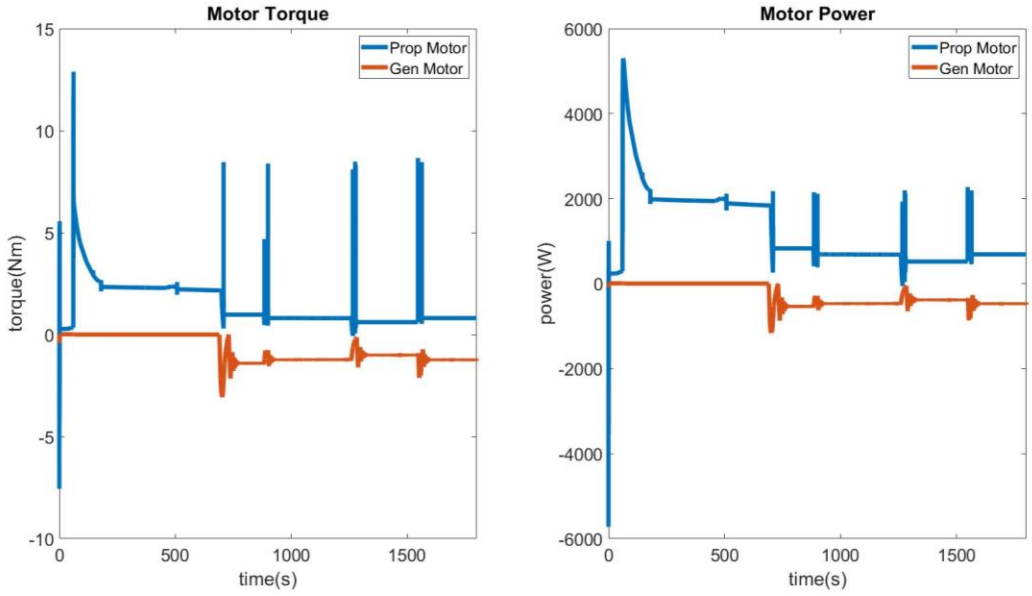

Figure 16 Motor/Generator power and torque results

The results from both the propulsive motor and generator show that during the take-off phase which lasts for approximately a 60s, the generator is not active and the propulsive motor experiences a large power spike as the aircraft takes flight and begins to climb. This large power request is a result of the requested rate of climb, which is set by the altitude profile to be 770ft/min at a speed of 30m/s. Following the initial spike, power settles to a reasonable value of about 2000 W, as the aircraft continues its climb at 30m/s with a quick speed increase to 35 m/s during the climb. After the climbing segment when the aircraft reaches the cruise altitude of 2500m still traveling at 35m/s, we see that the motor power is further reduced to approximately 1000W because the required power is less during cruise. Moreover, we see that the because the battery SOC has reduced to 60% during the climbing segment the generator is now producing power to match the propulsive power and while holding the battery SOC at the threshold value. Similar to the battery results, we see that spikes exist where the aircraft transitions to different speeds, which occurs in less than 60s. The spikes in power are observed when the aircraft is asked to accelerate to a different speed quickly.

Lastly, we can see that the IOL controller's ability to track the optimal BSFC trajectory (Figure 17) is not exactly in line with that shown in Figure 11. This figure shows the power and torque data points that the controller chose to operate at on the efficiency line. This behavior is possibly due to the low amount of data points used in the BSFC map for developing the ideal trajectory line. This lack of fidelity possibly did not allow for the capturing of the behavior engine at different throttle conditions or efficiency values. The resulting interpolation to obtain the required data values likely led to the controller deviating from the optimal BSFC trajectory. However, it is seen that, by design, the engine is controlled to operate in a very efficient region where BSFC is between 661- 706 g/kWh. Further refinement of the control logic and the BSFC map can lead to improved model performance.

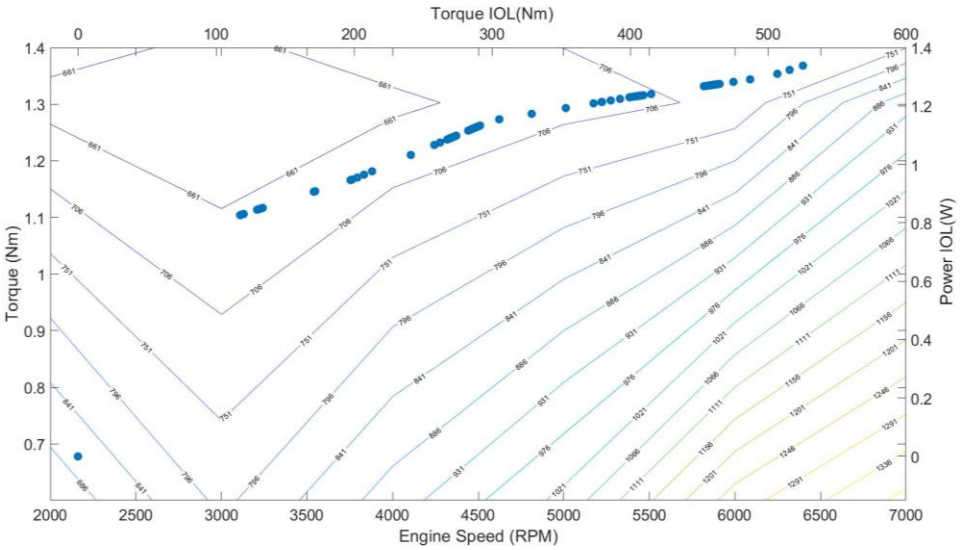

Figure 17 IOL controller tracking results

VI. Conclusion

Hybrid powertrains offer a significant improvement in performance, noise, fuel cost savings, and engine emissions in propulsion systems for unmanned aircraft. Current understanding of the performance benefits specific to different hybrid powertrain configurations is lacking. Furthermore, current knowledge is limited by a lack of dynamic powertrain models, which consider detailed performance maps for individual hardware components such as engines and electric motors. This work aims to use dynamic powertrain models for unmanned air systems to perform comparative performance analysis for different hybrid configurations. MATLAB/Simulink is used to construct a dynamic model of a series hybrid powertrain. The model is constructed using sub-models for the hardware component including the gasoline-fueled engine, a motor, a generator, a propeller and the aircraft itself. An ideal operating line (IOL) controller that optimizes engine fuel consumption is used to control the hybrid powertrain operation. The controller attempts to optimize engine fuel consumption by choosing engine operating points corresponding to generator power demand with the lowest brake specific fuel consumption. The IOL controller is aided in this process by an engine map providing torque, power, and fuel consumption values as measured for a suitable engine for the unmanned air system. Simulation results show the controller and the powertrain being capable of following the desired mission profile. The controller works as expected with the generator turning on when the threshold state of charge of the battery is reached. The engine-generator unit turns on as required to provide propulsive power and to maintain the desired state of charge of the battery. Some spikes in battery current and voltage and generator torque and power are observed, which correspond to transient events. While the IOL controller is observed to not exactly follow the ideal path on the specific fuel consumption curve, it is seen to maintain a fuel-efficient operation overall. Future efforts will focus on improvement in the controller logic as well as using engine performance maps with higher resolution to ensure an optimal path being followed by the controller. Other tasks include modeling of the more complex parallel and split power configurations, as well as the development of a hardware platform for testing hybrid powertrains.

Acknowledgments

This work was funded by the Air Force Research Laboratory through grant #FA 8650-18-2-2232. We would like to acknowledge the collaboration with James Benbrook and Dr. Christopher Hagen from the Oregon State University who provided engine performance data and KofiAgyemang Amankwah and Dr. Stephen Akwaboa from Southern University – Baton Rouge who provided inputs regarding the propeller model for this work. Further, we would like to acknowledge the discussion and inputs from Dr. Michael Rottmayer and Dr. Thomas Howell at the Air Force Research Laboratory.

References

[1] J. Schömann, "Hybrid-Electric Propulsion Systems for Small Unmanned Aircraft," *Doctoral dissertation, Technische Universität München,* 2014.

[2] A. Emadi, Advanced electric drive vehicles, CRC Press, 2014.

[3] Siemens, "Electric hybrid drives for aircraft," 9 July 2013. [Online]. Available: https://phys.org/news/2013-07-electric-hybrid-aircraft.html.

[4] U.S. Navy, *A Scan Eagle Unmanned Aerial Vehicle,* 2016.

[5] J. G. Herrera, J. A. Dechant and E. K. Green, "Technology Trends in Small Unmanned Aircraft Systems (sUAS) and Counter-UAS: A Five Year Outlook," Institute for Defense Analyses Alexandria, 2017.

[6] G. L. Soloveichik, "Battery technologies for large-scale stationary energy storage," *Annual review of chemical and biomolecular engineering,* vol. 2, pp. 503-527, 2011.

[7] M. Voskuijl, J. van Bogaert and A. . G. Rao, "Analysis and design of hybrid electric regional turboprop aircraft," *CEAS Aeronautical Journal,* vol. 9, no. 1, pp. 15-25, 2018.

[8] H. L. Silva and A. A. Gil, "Hybrid-electric aircraft: conceptual design, structural and aeroelastic analyses," 2017.

[9] A. T. Isikveren, C. Pornet, S. Kaiser and P. C. Vratny, "Pre-design strategies and sizing techniques for dual-energy aircraft," *Aircraft Engineering and Aerospace Technology,* pp. 525-542, 2014.

[10] S. P. Brown, "Design and Optimization of a 1 kW Hybrid Powertrain for Unmanned Aerial Vehicles," Oregon State University, 2017.

[11] S. Miller, "Hybrid-Electric Vehicle Model in Simulink," 2019.

[12] F. G. Harmon, "Neural network control of a parallel hybrid-electric propulsion system for a small unmanned aerial vehicle," University of California, 2005.

[13] J. Whidborne, "Calculating the lift-drag polar for the Aerosonde UAV using Chebfuns," 2016.

[14] J. Y. Hung and L. F. Gonzalez, "Design, simulation and analysis of a parallel hybrid electric propulsion system for unmanned aerial vehicles." Optimage Ltd., Brisbane C," *Proceedings of the 28th International Congress of the Aeronautical Sciences,* pp. 1-13, 2012.

[15] J. P. Gao, G. M. Zhu, E. G. Strangas and F. C. Sun, "Equivalent fuel consumption optimal control of a series hybrid electric vehicle," *Proceedings of the Institution of Mechanical Engineers, Part D: Journal of Automobile Engineering,* pp. 1003-1018, 2009.

[16] B. Messner and D. Tilbury, "Control Tutorials for MATLAB and Simulink - Motor Speed: System Modeling," 2018.